



HAL
open science

Altimetry of the Venus cloud tops from the Venus Express observations

Nikolay I. Ignatiev, Dmitry V. Titov, Giuseppe Piccioni, Pierre Drossart,
Wojciech J. Markiewicz, Valeria Cottini, Th. Roatsch, Miguel Almeida, N.
Manoel

► **To cite this version:**

Nikolay I. Ignatiev, Dmitry V. Titov, Giuseppe Piccioni, Pierre Drossart, Wojciech J. Markiewicz, et al.. Altimetry of the Venus cloud tops from the Venus Express observations. *Journal of Geophysical Research. Planets*, 2009, 114, 10.1029/2008JE003320 . hal-03786221

HAL Id: hal-03786221

<https://hal.science/hal-03786221>

Submitted on 24 Sep 2022

HAL is a multi-disciplinary open access archive for the deposit and dissemination of scientific research documents, whether they are published or not. The documents may come from teaching and research institutions in France or abroad, or from public or private research centers.

L'archive ouverte pluridisciplinaire **HAL**, est destinée au dépôt et à la diffusion de documents scientifiques de niveau recherche, publiés ou non, émanant des établissements d'enseignement et de recherche français ou étrangers, des laboratoires publics ou privés.

Copyright

Altimetry of the Venus cloud tops from the Venus Express observations

N. I. Ignatiev,^{1,2} D. V. Titov,² G. Piccioni,³ P. Drossart,⁴ W. J. Markiewicz,² V. Cottini,^{3,5} Th. Roatsch,⁶ M. Almeida,⁷ and N. Manoel^{2,8}

Received 16 December 2008; revised 17 March 2009; accepted 29 May 2009; published 13 August 2009.

[1] Simultaneous observations of Venus by Visible and Infrared Thermal Imaging Spectrometer and Venus Monitoring Camera onboard the Venus Express spacecraft are used to map the cloud top altitude and to relate it to the ultraviolet (UV) markings. The cloud top altitude is retrieved from the depth of CO₂ absorption band at 1.6 μm . In low and middle latitudes the cloud top is located at 74 ± 1 km. It decreases poleward of $\pm 50^\circ$ and reaches 63–69 km in the polar regions. This depression coincides with the eye of the planetary vortex. At the same latitude and hour angle, cloud top can experience fast variations of about 1 km in tens of hours, while larger long-term variations of several kilometers have been observed only at high latitudes. UV markings correlate with the cloud altimetry, however, the difference between adjacent UV dark and bright regions does not exceed several hundred meters. Surprisingly, CO₂ absorption bands are often weaker in the dark UV features, indicating that these clouds may be a few hundred meters higher or have a larger scale height than neighboring clouds. Ultraviolet dark spiral arms, which are often seen at about -70° , correspond to higher altitudes or to the regions with strong latitudinal gradient of the cloud top altitude. Cloud altimetry in the polar region reveals the structure that correlates with the thermal emission maps but is invisible in UV images. This implies that the UV optically thick polar hood is transparent in the near IR.

Citation: Ignatiev, N. I., D. V. Titov, G. Piccioni, P. Drossart, W. J. Markiewicz, V. Cottini, Th. Roatsch, M. Almeida, and N. Manoel (2009), Altimetry of the Venus cloud tops from the Venus Express observations, *J. Geophys. Res.*, 114, E00B43, doi:10.1029/2008JE003320.

1. Introduction

[2] A remote observer sees numerous features in the ultraviolet (UV) spectral range in the top layers of Venus's thick cloud deck. The nonuniform vertical and horizontal distribution of an unknown UV absorber produces contrast markings that have puzzled scientists since their discovery [Rossow *et al.*, 1980; Esposito, 1980]. Variations of temperature and cloud structure above the tropopause (~ 60 km) appear as specific features in the thermal infrared range [Taylor *et al.*, 1980]. These features indicate temperature conditions and processes at the cloud tops, but poor knowl-

edge of the altitude where they form makes their interpretation difficult. This uncertainty affects altitude assignment to the cloud tracked winds and trace gas abundances. The question of cloud top altitude is also directly related to the problem of location of the unknown UV absorber.

[3] Earlier observations provided several tools to determine the cloud top altitude (i.e., the altitude of unit cloud optical depth τ) and aerosol structure. The measurements of solar fluxes, spectra of scattered radiation, and aerosol microphysical properties by the Pioneer Venus and Venera descent probes enabled the construction of consistent models of particulate and optical properties of the cloud layer at low and middle latitudes [Esposito *et al.*, 1983; Tomasko *et al.*, 1985; Ragent *et al.*, 1985; Moroz *et al.*, 1985]. These models placed the $\tau \sim 1$ level in the visible range at about 70 km. Kawabata *et al.* [1980] and later Sato *et al.* [1996], Knibbe *et al.* [1998], and Braak *et al.* [2002] used the Pioneer Venus Orbiter Cloud Photopolarimeter (OCPP) observations to constrain the microphysical and optical properties and structure of the upper haze. They concluded that in the polar regions ($70\text{--}90^\circ\text{N}$) a submicron haze with radius $r \sim 0.25$ μm is responsible for UV opacity of ~ 0.8 above the main cloud which top is located at about 40 mbar (~ 68 km). In equatorial regions the submicron haze opacity is about an order of magnitude lower and the level $\tau \sim 0.8$

¹Space Research Institute for Russian Academy of Sciences, Moscow, Russia.

²Max Planck Institute for Solar System Research, Katlenburg-Lindau, Germany.

³INAF, IASF, Rome, Italy.

⁴LESIA, Observatoire de Paris, Meudon, France.

⁵Now at NASA Goddard Space Flight Center, Greenbelt, Maryland, USA.

⁶Institute of Planetary Research, German Aerospace Center, Berlin, Germany.

⁷ESA, ESAC, Madrid, Spain.

⁸Department of Mathematics, University of Évora, Évora, Portugal.

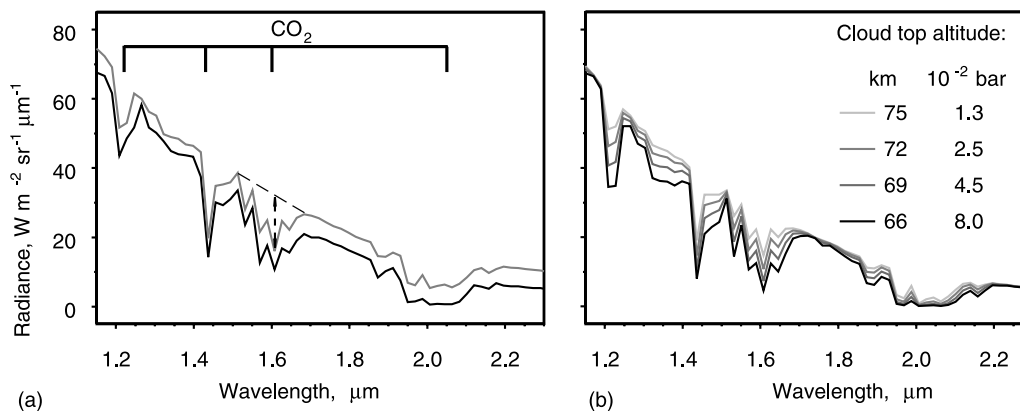


Figure 1. (a) VIRTIS-M measured (black) and synthetic (gray) spectra of the Venus dayside. The synthetic spectrum is shifted by $+5 \text{ W m}^{-2} \text{ sr}^{-1} \mu\text{m}^{-1}$. Dotted lines show continuum and band depth ($\text{continuum} - S(\lambda_D)$). Positions of CO_2 bands are shown. (b) Synthetic VIRTIS-M spectra calculated for several cloud top altitudes.

is located inside the main cloud layer at ~ 28 mbar (~ 70 km). Thus the OCPP observations implied that the cloud top is by about one atmospheric scale height lower in the polar regions than in low latitudes. Pioneer Venus radio occultation measurements showed that the cloud tops at the pole are 100 mbar deeper than those at the equator [Cimino *et al.*, 1980]. Thermal emission spectrometry onboard Venera-15 orbiter suggested also that the cloud top altitude at $\sim 1200 \text{ cm}^{-1}$ ($8.3 \mu\text{m}$) descends from ~ 70 km in low latitudes to ~ 60 km in the polar region [Zasova *et al.*, 2007].

[4] Imaging of Venus simultaneously in the near-IR by Visible and Infrared Imaging Spectrometer (VIRTIS) [Drossart *et al.*, 2007] and in the UV range ($0.365 \mu\text{m}$) by Venus Monitoring Camera (VMC) [Markiewicz *et al.*, 2007a] onboard Venus Express [Svedhem *et al.*, 2007; Titov *et al.*, 2006] provides a novel tool to determine the cloud top altitude and its variations over the planet and allows one to correlate them with observed UV features. Here we present the results of the cloud top altimetry investigations using the VIRTIS mapping in the $1.6 \mu\text{m}$ band of CO_2 .

2. Observations

[5] On 11 April 2006 Venus Express was inserted in a polar orbit around Venus, and few months later it began nominal science operations [Svedhem *et al.*, 2007]. Nadir observations from apocenter and in ascending branch of the orbit provide global imaging of the planet [Titov *et al.*, 2006]. VIRTIS takes the images and mosaics (VIRTIS-M channel) of the Venus disc in a broad spectral range from UV ($0.3 \mu\text{m}$) to thermal infrared ($5 \mu\text{m}$) with a spectral resolution in the IR of ~ 15 nm, as well as high-resolution spectra (VIRTIS-H channel) in the interval of $2\text{--}5 \mu\text{m}$ with the spectral resolution of $\sim 1\text{--}3$ nm [Drossart *et al.*, 2007]. A VIRTIS-M image has 256 elements (pixels) in the direction along the slit of the spectrometer. In some measurement sequences 256 pixels are binned in groups of 4 pixels to give 64 elements in the image. Scanning in the direction normal to the slit gives an image. A typical size of the VIRTIS-M images is about 4000×4000 km at apocenter, decreasing as the spacecraft approaches the planet [Piccioni *et al.*, 2007]. For each spatial element of

~ 20 km and smaller VIRTIS-M near-IR spectra were used to derive the cloud top altitude. VMC performs simultaneous observations in the narrow-band filter at $0.365 \mu\text{m}$ with spatial resolution of 50 km or better, thus providing full-disc context images of the Venus cloud tops in the spectral band of the unknown UV absorber [Markiewicz *et al.*, 2007b].

[6] We processed 840 dayside VIRTIS-M measurement sequences with the exposure time of 20 and 300 ms taken on 120 orbits from the beginning of the mission up to orbit 853, from April 2006 to August 2008. Dayside of the southern hemisphere is completely covered by the VIRTIS-M observations, while on the dayside of the northern hemisphere VIRTIS-M image footprints look like narrow stripes. The number of such observation sessions is also limited. The lack of the data in the northern hemisphere can be compensated with the VIRTIS-H measurements, which have been analyzed by Cottini *et al.* [2008]. Here we also used VIRTIS-H data for cross check of the results.

[7] The VIRTIS instrument is optimized for observations of the nightside of the planet. Dayside spectral intensities are several orders of magnitude more intense than those for the nightside, and contain a sawtooth odd/even spectel (spectral element) component, which was not completely removed by the calibration procedure. For this reason, here we used an undersampled spectrum composed of odd spectels only (Figure 1). The spectral resolution appeared to be a bit worse than the nominal value obtained in the preflight laboratory calibrations. The instrumental function of the VIRTIS-M used here was represented by a Gaussian curve with the FWHM of 15 nm at $1.6 \mu\text{m}$.

3. Method of the Cloud Top Altitude Determination

[8] Spectrum of the solar radiation reflected from the dayside of Venus shows several strong CO_2 absorption bands in the near IR range (Figure 1). Their relative depth increases with the total number of CO_2 molecules on the line of sight and, thus, depends on the effective path of radiation in the atmosphere. This path is a function of the cloud altitude, its vertical structure, aerosol optical proper-

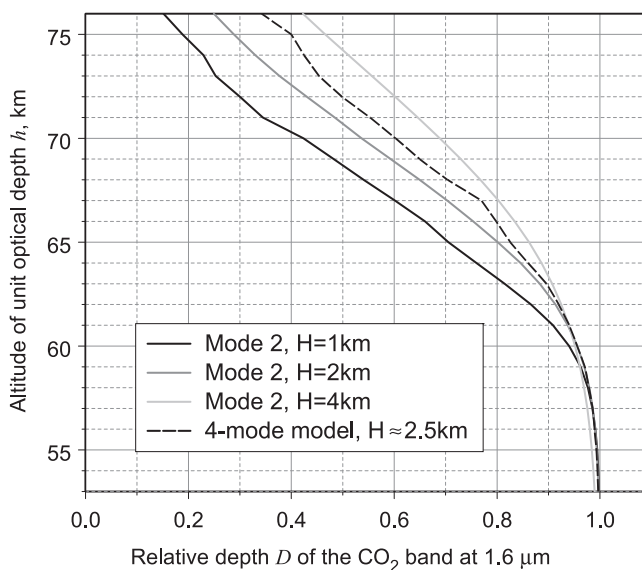


Figure 2. Modeled dependence of the CO₂ 1.6 μm normalized band depth index on the cloud top altitude for different cloud structure/scale heights.

ties, atmospheric temperature and pressure, and geometry of observations. Using the depths of CO₂ bands and some assumptions about properties and atmospheric parameters, the vertical structure of the clouds can be evaluated. Here we use an exponential model of aerosol vertical distribution with two parameters: cloud top altitude h , defined as the altitude of unit optical depth at 1.51 μm, and aerosol scale height H . We adopted the temperature and pressure profiles from the Venus International Reference Atmosphere (VIRA) model [Seiff *et al.*, 1985] and assumed cloud particles composed of 75% sulfuric acid with complex refraction index from Palmer and Williams [1975]. Particle size distribution was represented by “mode 2,” i.e., log-normal function with $r_m = 1.05$ μm and $\sigma = 1.21$ [Pollack *et al.*, 1980]. These assumptions are evident simplifications: both temperature profile and particle size distribution in the region of cloud tops vary with latitude [e.g., Ragent *et al.*, 1985; Zasova *et al.*, 2007]. However, the effect of a variable temperature profile on the dayside reflectance spectrum is much weaker than that owing to cloud top pressure variations. The submicron haze dominating at higher altitudes is almost transparent in the IR. Larger mode 3 particles can sometimes dominate the aerosol population at the cloud top at high latitudes, but substituting them with equivalent number of mode 2 particles would just slightly bias the measured cloud top altitude. However, we also tested the retrievals with complete 4-modal particle size distribution (Figure 2). To characterize the relative depth of CO₂ band, we define the depth index D as difference between the continuum $cont(\lambda_D)$ and the spectrum inside the band $S(\lambda_D)$ normalized to the continuum at wavelength λ_D :

$$D = \frac{cont(\lambda_D) - S(\lambda_D)}{cont(\lambda_D)},$$

where $\lambda_D = 1.61$ μm, and the continuum is defined by a straight line drawn between the two points on the sides of the band: 1.51 and 1.70 μm.

[9] Synthetic spectra were calculated for a discrete set of parameters $(h, H, \mu_0, \mu, \varphi)$, where μ_0 and μ are the cosines of the zenith angles of incident and outgoing radiation, and φ is the relative azimuth angle of the outgoing radiation. This yielded 5-dimensional matrix $D = D(h, H, \mu_0, \mu, \varphi)$ that was used in the analysis of VIRTIS spectra. Our radiative transfer model is based on the discrete ordinate code DISORT [Stamnes *et al.*, 1988] coupled with a line-by-line model of gaseous absorption. CO₂ line parameters were taken from the preliminary version of Carbon Dioxide Spectroscopic Database (CDSD) for Venus (S. A. Tashkun and V. I. Perevalov, personal communication, 2007) which is available at the anonymous ftp site of Institute of Atmospheric Optics of Russian Academy of Sciences (<ftp://ftp.iao.ru/pub/Venus>), the CO₂ high-temperature database [Pollack *et al.*, 1993], and HITRAN (<http://www.hitran.com>). Data on other gases (CO, H₂O) were taken from HITRAN [Rothman *et al.*, 2005], version of 2006. Voigt line profiles were used. For CO₂, the line profile was multiplied by a sub-Lorentzian χ factor [Pollack *et al.*, 1993, equations 1–4].

[10] Figure 2 shows the dependence of the computed band depth index D on the cloud top altitude for the simplified mode 2 cloud model and three values of the aerosol scale height. It is compared to the complete 4-mode cloud model by Pollack *et al.* [1980], with modifications by Zasova *et al.* [1985], which around the altitude of the unit optical depth has $H \sim 2.5$ km. Determination of both aerosol scale height and cloud top altitude using one wavelength is ambiguous. The same band depth index D may be obtained with lower clouds having sharp upper boundary ($H = 0$) and with higher clouds that are more diffuse (i.e., large H). Radiation in the center and in the wings of CO₂ bands comes from the levels separated by few kilometers enabling us, in principle, to derive both parameters from the spectrum. Earlier observations indicated that the cloud scale height at the cloud tops can vary from less than 1 km in some regions at high latitudes [Zasova *et al.*, 1993, 2007] to 4–5 km at the equator [Ragent *et al.*, 1985; Zasova *et al.*, 1993, 2007; Koukoulis *et al.*, 2005]. However, this behavior does not follow from our data: both low- and high-latitude spectra were better fitted with the scale height of 4–6 km. We concluded that a reliable determination of at least two parameters requires improvements in the fit of the whole band or several bands and therefore improvements in the spectral and radiometric calibration. In the absence of these improvements, we assumed a constant scale height of 4 km, being a reasonable value for low and middle latitudes and allowing us to perform first-order cloud height determinations. An uncertainty that follows from this assumption is considered below.

[11] Once the scale height is fixed, monotonic dependence of the band depth on the cloud top altitude makes the solution of the inverse problem straightforward. For each VIRTIS-M spectrum, we interpolate the function $D = D(h, H, \mu_0, \mu, \varphi)$ given by the precalculated 5-dimensional matrix to the actual values of H, μ_0, μ, φ , thus defining function $D(h)$ on a set of discrete h levels. Interpolation of inverse function $h(D)$ gives h that corresponds to the measured value of D (Figure 2).

[12] The principal uncertainty of our approach results from the assumption about the constant scale height of

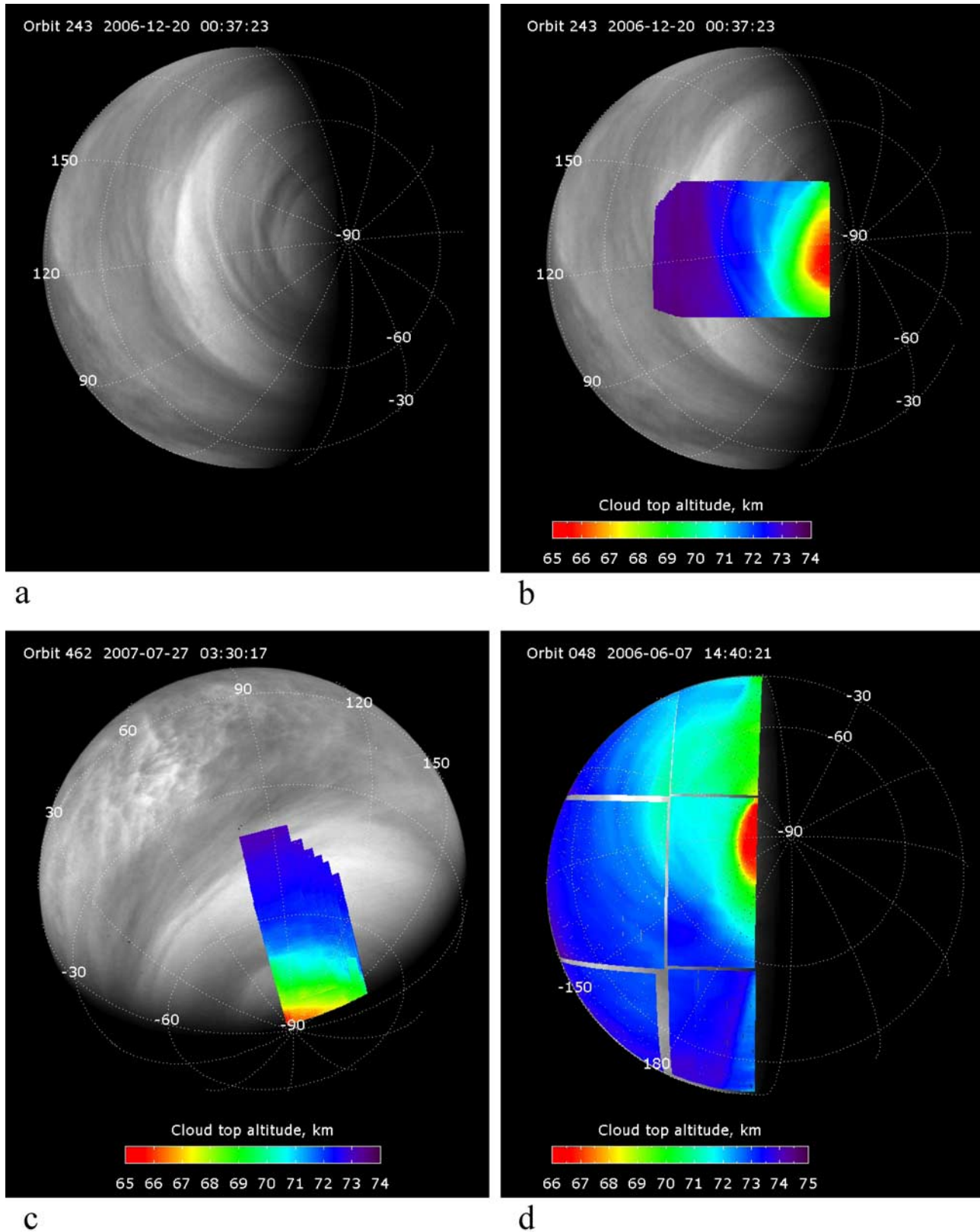


Figure 3. Venus Monitoring Camera ultraviolet (VMC UV) images with overplotted cloud altimetry maps for orbits (a and b) 243, (c) 462, and (d) 48. Note correlation of the cloud altimetry and UV dark and bright features.

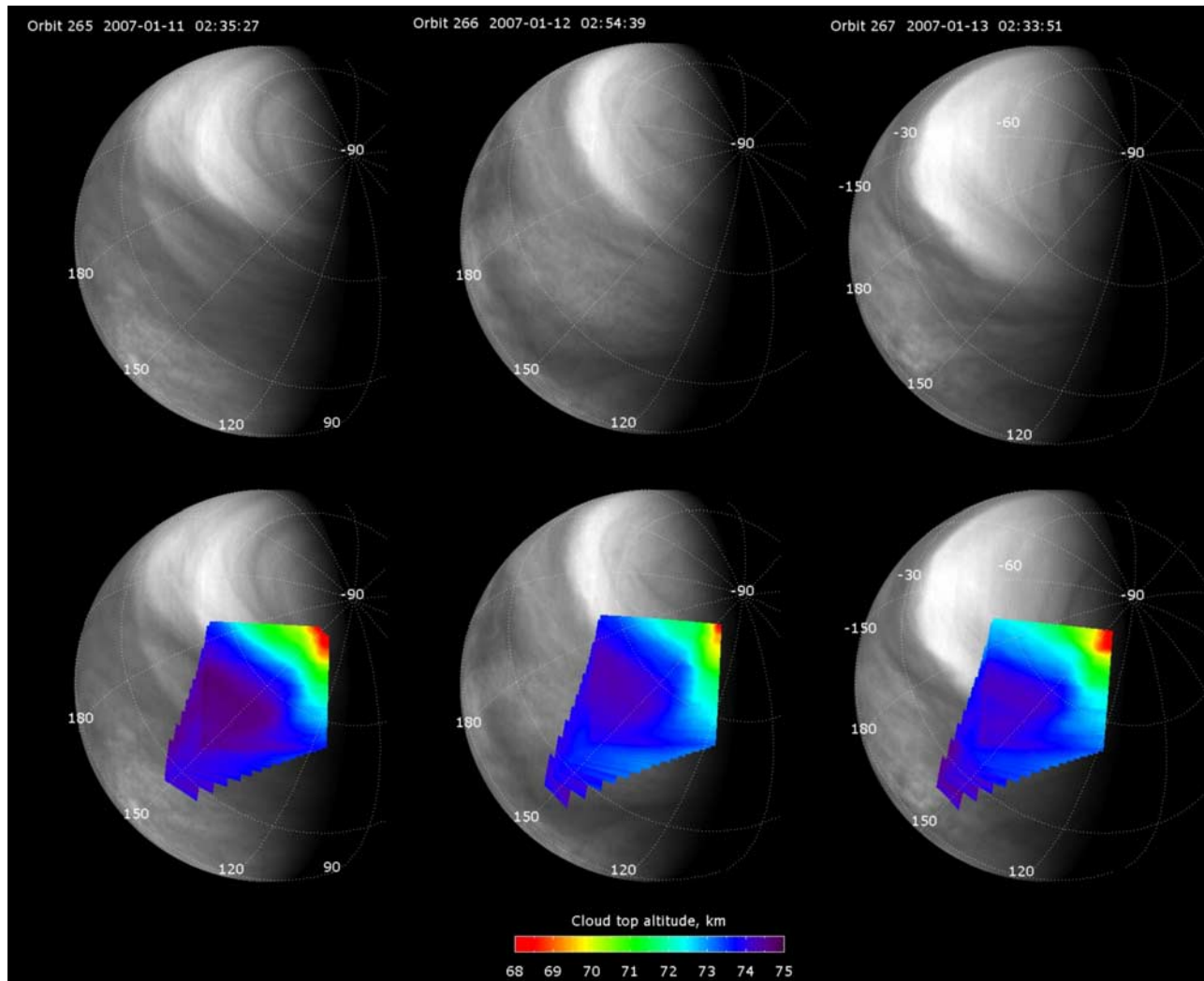


Figure 4. Cloud altimetry and UV images for three consecutive orbits during the polar brightening event.

4 km. For low clouds (~ 65 km) the altitude uncertainty corresponding to the scale height range from 1 to 5 km is equal to 4 km, while for high clouds (75 km) it increases up to 6 km (Figure 2). Smaller scale heights result in lower cloud top altitudes. However, large variations of scale height values are encountered only in high latitudes [Zasova *et al.*, 1993, 2007]. Assuming that possible variations of the scale height in low latitudes are equal to 3–5 km and in high latitudes to 1–5 km, we may evaluate this uncertainty as ± 1.5 km and $+1/-3$ km in low and high latitudes, respectively. Another systematic bias is caused by a single temperature and pressure vertical profile used in our model. At high latitudes the level of 100 mb is located by $\sim 1-2$ km lower than that at low latitudes [Seiff *et al.*, 1985; Zasova *et al.*, 2006], which means that at high latitudes our results should be corrected by $-1-2$ km.

[13] Instrument calibration uncertainties resulted in the dependence of the measured band depth on sample number (position of a pixel in the direction along the slit). It can be caused by imperfect flat fielding and spectral calibration. These two effects are difficult to separate. The above defined matrix D was calculated assuming fixed positions

of spectral channels, which actually depend on temperature of the instrument and sample number. Variations of a spectral wavelength around the average value can be ± 0.5 spectral size (9.5 nm). Interpolation of the measured spectrum to the predefined set of wavelengths introduces an error evaluated as a few hundred meters. A similar effect is caused by a systematic shift of the wavelength scale present in the calibrated data. Despite the systematic behavior of the shift, we found it difficult to evaluate with a precision better than ± 0.2 spectral size because of the odd-even spectral problem, spectral resolution uncertainty, and other factors that might cause residual differences between measured and synthetic spectra. The total uncertainty of this kind expressed in terms of the retrieved cloud top altitude is evaluated as ± 1 km and will be illustrated in section 4 (Figures 3d and 7b). On some orbits where the images taken with 20 ms exposure were interleaved with those of 300 ms, we detected a difference up to several hundred meters in the cloud top altitudes derived from the adjacent measurement sessions.

[14] Provided the model and data calibration are perfect, any other reasonable choice of spectral bands or channels used to derive the cloud top altitude should lead us to

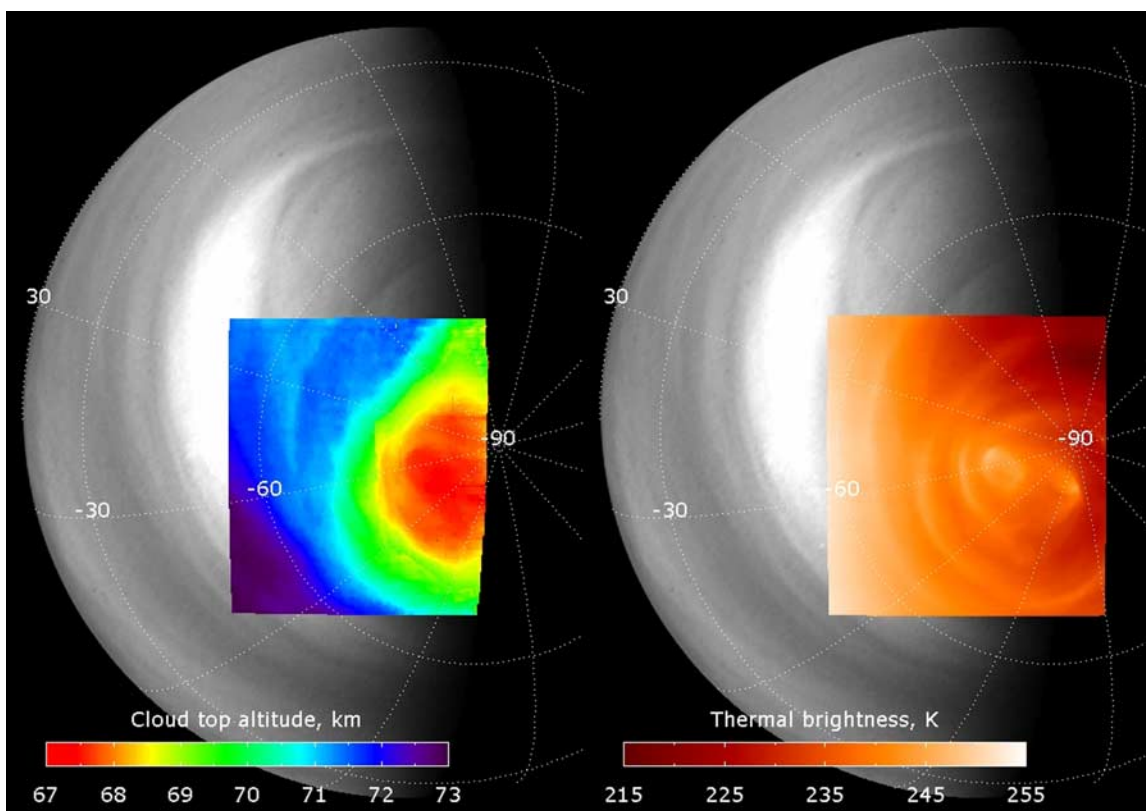


Figure 5. Comparison of the (left) cloud top altimetry with (right) thermal IR ($5 \mu\text{m}$) VIRTIS image, both overlotted on the simultaneously captured VMC UV image (orbit 674).

similar results. We have demonstrated this using a longer wavelength band observed by the VIRTIS-H channel (see section 4). An alternative to the relative band depth index D is the traditional equivalent width of the band. We found that using the latter value moves down the retrieved cloud top altitude by ~ 1 km.

[15] Summarizing all the uncertainties we conclude that the absolute precision of the cloud top measurement does not exceed 2 km at low and middle latitudes. At high latitudes a lower-altitude error limit should be extended by another 2 km. For a single pixel, the relative precision limited by the sensitivity of the spectrum to the cloud top variations and the instrumental noise is few hundred meters for 20 ms exposure time, and tens of meters for 300 ms.

4. Results and Discussion

[16] The first results on the global cloud top altimetry were reported by Titov *et al.* [2008]. Here we applied routinely the above described method to the VIRTIS-M dayside observations. Typical examples of the cloud top altimetry maps are shown in Figure 3. The mosaics consist of overlapping VIRTIS-M images taken at ascending branch of the orbit while the field of view moved from the South pole to the middle latitudes (Figures 3b and 3c) or global mosaics that completely covered the Southern hemisphere (Figure 3d). The altimetry maps are overlotted on the simultaneously taken VMC UV image that allowed us to relate the cloud top altitude to the UV markings. Some altimetry maps, whenever necessary, are processed with a

simple median filter with a window size up to 11 pixels in the direction along the slit and up to 5 pixels in the perpendicular direction to improve the image quality at the minimum degradation of spatial resolution.

[17] The cloud top is located at remarkably constant altitude of 74 ± 1 km over most of the planet (Figure 3). Poleward from 50 to 60 degrees latitude the cloud top quickly descends reaching its minimum of 65–68 km in the huge polar depression 2000–3000 km in size. The elevation change from equator to pole is about 1–2 atmospheric scale heights. The general trend is quite typical and is reproduced from orbit to orbit within 1 km. Variations of that magnitude at a given latitude and solar hour angle may occur on time scales of tens of hours and can be sometimes clearly seen when comparing images taken at the same geometry from consecutive orbits and therefore separated by 24 h (e.g., Figure 4).

[18] The global pattern did not change much during the polar brightening event that occurred on 13 January 2007 [Markiewicz *et al.*, 2007b] when both brightness and latitude extension of the polar hood significantly increased for a few days (Figure 4). Surprisingly, these drastic changes in UV appearance had no considerable effect on the cloud top altitude derived from the VIRTIS near-IR spectra: their changes were within the limits of usual variations of 1–2 km. Also surprising is that the sharp boundary between the UV dark low latitudes and bright midlatitudes is not pronounced in the cloud altimetry maps (Figure 4). This implies that the UV brightening was not associated with significant changes in cloud top altitude.

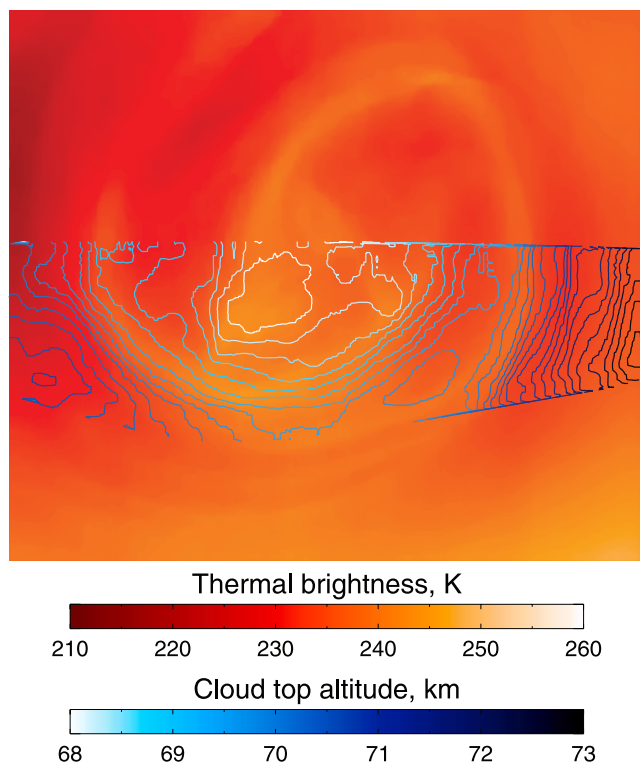


Figure 6. Correlation of the fine structure of the vortex eye (orange image, $5 \mu\text{m}$) with the cloud top pattern (blue isolines). Altimetry data are absent in the nightside (top) and in a bright region of the dayside (bottom), where the signal is saturated at 300 ms exposure. Contours are drawn every 0.2 km starting from 67.8 km in the center.

This also means that either the thickness of the bright UV hood does not exceed few hundred meters or that the hood is transparent at thermal IR wavelengths, the latter indicating that it consists of submicron particles. *Markiewicz et al.* [2007b] tentatively explained the brightening event by quick formation of fine sulfuric acid haze by homogeneous nucleation and its clearing due to coagulation decay of aerosol number density.

[19] UV dark spiral and circular features usually present at -70° are clearly seen in the cloud altimetry maps as variations of several hundred meters on the global slope to the pole (Figures 3a and 3b). Contrary to the analysis of the Pioneer Venus polarization measurements [*Esposito and Travis, 1982*], these dark features are either located higher than the adjacent UV bright clouds (e.g., Figure 3b) or characterized by a higher latitudinal gradient of the cloud top altitude (e.g., Figure 3c).

[20] The polar depression in the cloud tops always coincides with the vortex eye observed by VIRTIS at thermal IR wavelength (Figure 5) [*Piccioni et al., 2007*]. The eye, which usually appears almost featureless in the UV (e.g., Figure 3a), shows complex patterns in the cloud altimetry maps that show high correlation with the thermal IR images at $5 \mu\text{m}$ (Figure 6). Hot spiral arms, which have almost the same temperature as the core, are located higher than it and characterized by the strong gradient of the cloud top altitude, thereby being the boundary of the polar vortex.

[21] We analyzed 545 VIRTIS frames taken with 20 ms exposure in 72 orbits from the beginning of the mission till orbit 858 (April 2006 to August 2008). We averaged all analyzed data except for high emission angles ($\theta > 85^\circ$), where our plane parallel radiative transfer model is no longer valid. Figure 7 shows mean map of the cloud top altitude derived from this data set. On average, the cloud tops in middle and low latitudes are located at a constant altitude of ~ 74 km with orbit-to-orbit variations of about 1 km. Note that uncertainties discussed above can result in a systematic shift of this altitude by 1–2 km. Figure 7 shows no considerable local time dependence of the cloud top altitude, except for tentative indication of slightly higher altitudes in the afternoon at low latitudes, that coincides with the region of strongest convective activity observed by VMC [*Markiewicz et al., 2007b*].

[22] Since the Venus Express orbit is fixed in inertial space, optimal conditions for dayside observations at ascending branch of the orbit are naturally grouped in ~ 100 orbits interleaved with the same number of orbits devoted to nightside observations. This makes continuous monitoring of the cloud altitudes impossible. After orbit 610 we observed a systematic raise of the cloud tops at high latitudes by ~ 3 km with respect to orbits before the gap 505–609 in the dayside observations. Figure 8a compares the mean latitude trend derived from the first 500 orbits to that observed after the orbit 610. After scrutinizing the data and VIRTIS behavior we exclude instrumental effects and conclude that polar clouds can show strong long-term variability, as known from previous observations in the UV [*Kawabata et al., 1980; Esposito et al., 1988*].

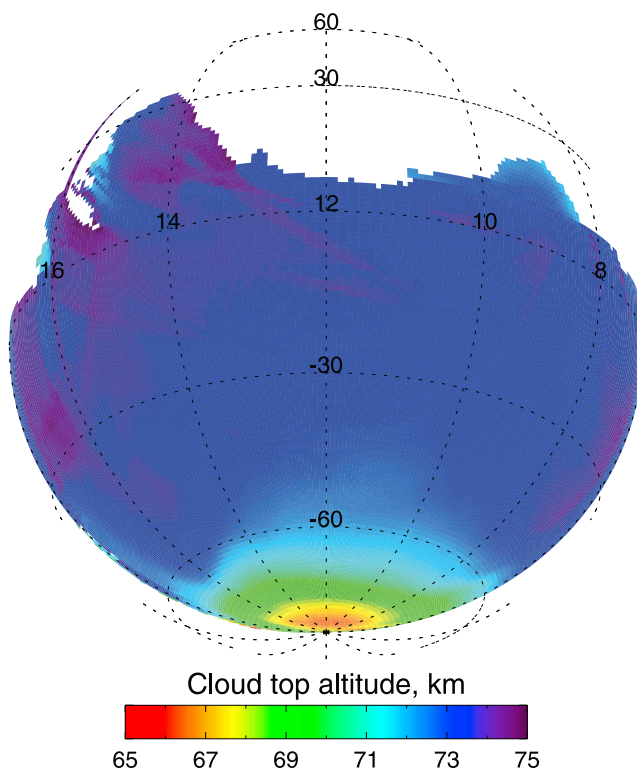


Figure 7. Mean cloud top altitude as a function of latitude and local time. Linear patterns are the traces of VIRTIS-M image frames.

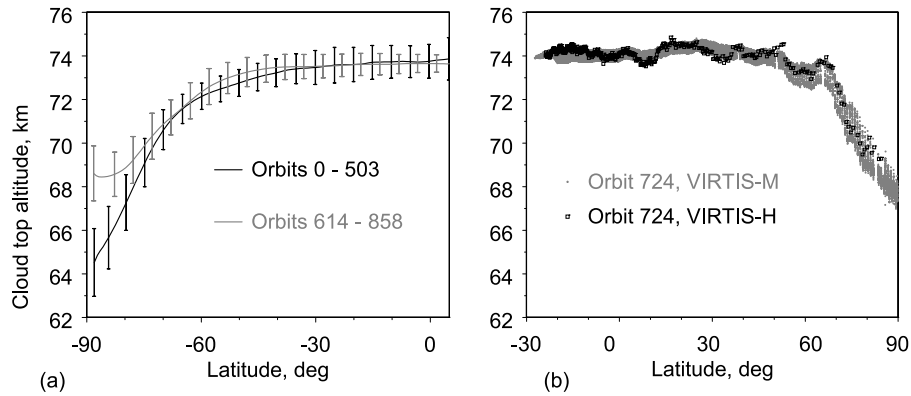


Figure 8. Latitudinal behavior of the cloud top altitude. (a) Mean value in the southern hemisphere for two periods: from April 2006 to September 2007 (orbits 0–503) (black) and from December 2007 to August 2008 (orbits 614–858) (gray). The curves are moving averages with 5° latitude window. Error bars represent scattering of individual measurements due to both temporal variations and instrumental errors. (b) Observations in the northern hemisphere in orbit 724 with by VIRTIS-M (dots) and VIRTIS-H (squares).

[23] Relatively random VIRTIS-M observations that passed over the northern hemisphere showed no principal difference in the cloud altimetry between the north and the south (Figure 8). Simultaneous VIRTIS-H measurements in orbit 724 allowed us to evaluate independently the cloud top altitudes from the weak CO_2 band at $2.5 \mu\text{m}$. Figure 8b demonstrates good agreement between both data sets. The VIRTIS-H cloud top altitudes shown in Figure 8b, although derived from $2.5 \mu\text{m}$ band, are referenced to $1.51 \mu\text{m}$ for comparison with the VIRTIS-M results. In the northern hemisphere, owing to a small distance to the planet, the VIRTIS-M image footprint on the clouds is a $\sim 50 \text{ km}$ wide stripe stretched along meridian from equator to pole (similarly, VIRTIS-H measurements cover a $\sim 3 \text{ km}$ wide stripe approximately in the center of the VIRTIS-M footprint). The scatter of the VIRTIS-M data points in Figure 8b is thus caused by the flat field and spectral calibration errors in the direction along the slit rather than the cloud altitude variability, which gives us an estimate of the effects of those errors on the results. The same effect appears as the difference between the adjacent frames in Figure 3d.

[24] The above described method provides the altitude of the $\tau = 1$ level at $1.5 \mu\text{m}$. We studied the relation between the cloud top altimetry derived from the near-IR observations and altitude of the UV markings. Optical properties of the submicron haze with $r_m \sim 0.15\text{--}0.25 \mu\text{m}$ are quite different from those of the main cloud in which the particles with $1\text{--}1.4 \mu\text{m}$ dominate. The extinction coefficient of the submicron haze in UV is several times greater than that in the near-IR. Thus the upper haze is almost transparent at $\sim 1.5 \mu\text{m}$, and at these wavelengths VIRTIS sounds the main cloud deck all over the planet. Calculations of the altitude of the unit optical depth level in the broad spectral range using the standard 4-modal aerosol distribution by Pollack *et al.* [1980] with low-latitude number density profiles by Zasova *et al.* [1985] show that the cloud top in UV is located almost at the same altitude as in the near-IR (Figure 9). This is representative of low and middle latitudes where the upper haze is generally of low density. Doubling

the number of submicron particles lifts the UV cloud top by $\sim 1 \text{ km}$. To simulate polar clouds we removed mode 2 particles, so that the main cloud deck is now composed of larger mode 2' particles and located below 65 km . It is overlaid by submicron upper haze with opacity of ~ 1 . In this case there is a significant difference of several kilometers between the levels of unit τ in the near IR and UV. This condition is often observed at high latitudes, where the UV opacity of submicron upper haze can reach ~ 0.8 [Kawabata *et al.*, 1980]. We note that Markiewicz *et al.* [2007b] estimated UV opacity to be of ~ 1 and haze vertical extension of $\sim 2 \text{ km}$ from the analysis of the brightening event (Figure 4).

[25] Simultaneous observations by the VIRTIS and VMC instruments onboard Venus Express provide an opportunity to assign altitudes to mesoscale UV markings and to

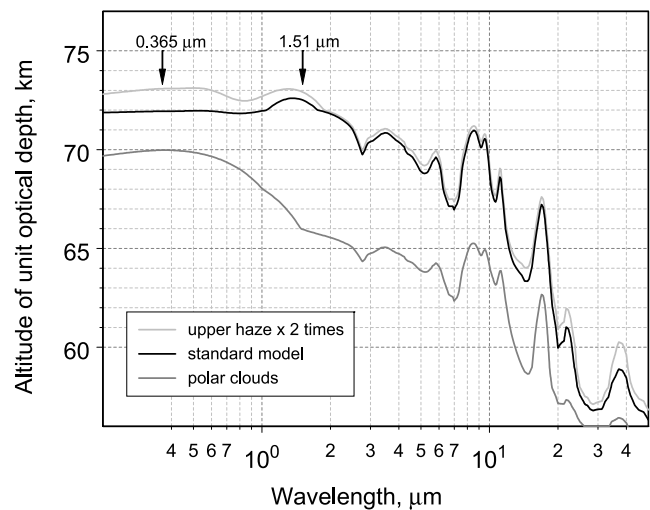


Figure 9. Cloud top altitude as a function of wavelength for the low-latitude 4-mode model of Venus clouds, the same model with the upper haze enhanced by 2 times, and the polar cloud model.

constrain location of the unknown absorber that produces these markings within the cloud deck. Surprisingly the analysis shows that the formal cloud top altitude increases in UV dark features. This relation is clearly seen in the region of dark spiral arms (Figures 3a–3b) in high latitudes. Such behavior, although obvious in the VIRTIS altimetry, contradicts the earlier observations suggesting that the UV absorber is located within the main cloud layer [Esposito and Travis, 1982; Esposito et al., 1983]. There are several possible explanations of this disagreement. First, Pioneer Venus and Venus Express observations were focused on different latitudes: from low to middle and from middle to high, respectively. Another plausible explanation is that our simple model description of the clouds is insufficient and should include variations of the cloud scale height and optical properties of the medium rather than the cloud top altitude only. In any case cloud top altitude variations related to dark UV markings do not exceed few hundred meters.

5. Conclusions

[26] Analysis of the VIRTIS and VMC observations showed that they provide a powerful tool to determine the cloud top altitude. These measurements assign the altitude of the cloud tracked winds and constrain the location of the unknown UV absorber with the cloud. Further investigations should include the feasibility study of the simultaneous scale height evaluation using several CO₂ IR absorption bands, and detailed cloud altimetry measurements at higher spatial resolution.

[27] **Acknowledgments.** Venus Express is a mission of the European Space Agency. We thank the Agenzia Spaziale Italiana (ASI) and the Centre National d'Études Spatiales (CNES) for the support and funding of the VIRTIS experiment. We gratefully thank all members of the Venus Express project and of the VIRTIS and VMC technical teams. N.I. was supported by the Russian Foundation of Basic Research grant 08-02-01383. We thank L.W. Esposito, R.W. Carlson, and an anonymous reviewer for their valuable comments that greatly helped us to improve the manuscript.

References

- Braak, C. J., J. F. de Haan, J. W. Hovenier, and L. D. Travis (2002), Spatial and temporal variations of Venus haze properties obtained from Pioneer Venus Orbiter polarimetry, *J. Geophys. Res.*, *107*(E5), 5029, doi:10.1029/2001JE001502.
- Cimino, J. B., C. Elachi, A. J. Kliore, D. J. McCleese, and I. R. Patel (1980), Polar cloud structure as derived from the Pioneer Venus Orbiter, *J. Geophys. Res.*, *85*(A13), 8082–8088, doi:10.1029/JA085iA13p08082.
- Cottini, V., N. Ignatiev, D. Grassi, G. Piccioni, and P. Drossart (2008), Venus mesospheric water vapor from VIRTIS-H VEX dayside measurements, *Eos Trans. AGU*, *89*(53), Fall Meet. Suppl., Abstract #P33A-1429.
- Drossart, P., et al. (2007), Scientific goals for the observation of Venus by VIRTIS on ESA/Venus express mission, *Planet. Space Sci.*, *55*, 1653–1672, doi:10.1016/j.pss.2007.01.003.
- Esposito, L. W. (1980), Ultraviolet contrasts and the absorbers near the Venus cloud tops, *J. Geophys. Res.*, *85*(A13), 8151–8157, doi:10.1029/JA085iA13p08151.
- Esposito, L. W., and L. D. Travis (1982), Polarization studies of the Venus UV contrasts: Cloud height and haze variability, *Icarus*, *51*, 374–390, doi:10.1016/0019-1035(82)90090-2.
- Esposito, L. W., R. G. Knollenberg, M. Ia. Marov, O. B. Toon, and R. P. Turco (1983), The clouds are hazes of Venus, in *Venus*, edited by D. M. Hunten et al., pp. 484–564, Univ. of Ariz. Press, Tucson.
- Esposito, L. W., M. Copley, R. Eckert, R. Gates, A. I. F. Stewart, and H. Worden (1988), Sulfur dioxide at the Venus cloud tops, 1978–1986, *J. Geophys. Res.*, *93*(D5), 5267–5276, doi:10.1029/JD093iD05p05267.
- Kawabata, K., D. L. Coffeen, J. E. Hansen, W. A. Lane, M. Sato, and L. D. Travis (1980), Cloud and haze properties from Pioneer Venus polarimetry, *J. Geophys. Res.*, *85*(A13), 8129–8140, doi:10.1029/JA085iA13p08129.
- Knibbe, W. J. J., J. F. De Haan, J. W. Hovenier, and L. D. Travis (1998), Analysis of temporal variations of the polarization of Venus observed by Pioneer Venus Orbiter, *J. Geophys. Res.*, *103*(E4), 8557–8574, doi:10.1029/98JE03558.
- Koukoulis, M. E., P. G. J. Irwin, and F. W. Taylor (2005), Water vapor abundance in Venus' middle atmosphere from Pioneer Venus OIR and Venera 15 FTS measurements, *Icarus*, *173*, 84–99, doi:10.1016/j.icarus.2004.08.023.
- Markiewicz, W. J., et al. (2007a), Venus Monitoring Camera for Venus Express, *Planet. Space Sci.*, *55*, 1701–1711, doi:10.1016/j.pss.2007.01.004.
- Markiewicz, W. J., D. V. Titov, S. S. Limaye, H. U. Keller, N. Ignatiev, R. Jaumann, N. Thomas, H. Michalik, R. Moissl, and P. Russo (2007b), Morphology and dynamics of the upper cloud layer of Venus, *Nature*, *450*, 633–636, doi:10.1038/nature06320.
- Moroz, V. I., A. P. Ekonomov, B. E. Moshkin, H. E. Revercomb, L. A. Sromovsky, J. T. Schofield, D. Spaenkuch, F. W. Taylor, and M. G. Tomasko (1985), Solar and thermal radiation in the Venus atmosphere, *Adv. Space Res.*, *5*(11), 197–232, doi:10.1016/0273-1177(85)90202-9.
- Palmer, K. F., and D. Williams (1975), Optical constants of sulfuric acid: Application to the clouds of Venus?, *Appl. Opt.*, *14*, 208–219.
- Piccioni, G., et al. (2007), South-polar features similar to those near the north pole, *Nature*, *450*, 637–640, doi:10.1038/nature06209.
- Pollack, J. B., O. B. Toon, R. C. Witten, R. Boese, B. Ragent, M. Tomasko, L. Esposito, L. Travis, and D. Wiedman (1980), Distribution and source of the UV absorption in Venus' atmosphere, *J. Geophys. Res.*, *85*(A13), 8141–8150, doi:10.1029/JA085iA13p08141.
- Pollack, J. B., et al. (1993), Near-infrared light from Venus' nightside: A spectroscopic analysis, *Icarus*, *103*, 1–42, doi:10.1006/icar.1993.1055.
- Ragent, B., L. W. Esposito, M. G. Tomasko, M. Y. Marov, V. P. Shari, and V. N. Lebedev (1985), Particulate matter in the Venus atmosphere, *Adv. Space Res.*, *5*(11), 85–115, doi:10.1016/0273-1177(85)90199-1.
- Rosow, W. B., A. D. Del Genio, S. S. Limaye, L. D. Travis, and P. H. Stone (1980), Cloud morphology and motions from Pioneer Venus images, *J. Geophys. Res.*, *85*(A13), 8107–8128, doi:10.1029/JA085iA13p08107.
- Rothman, L. S., et al. (2005), The HITRAN 2004 molecular spectroscopic database, *J. Quant. Spectrosc. Radiat. Transfer*, *96*, 139–204, doi:10.1016/j.jqsrt.2004.10.008.
- Sato, M., L. D. Travis, and K. Kawabata (1996), Photopolarimetry analysis of the Venus atmosphere in polar regions, *Icarus*, *124*, 569–585, doi:10.1006/icar.1996.0231.
- Seiff, A., J. T. Schofield, A. J. Kliore, F. W. Taylor, S. S. Limaye, H. E. Revercomb, L. A. Sromovsky, V. V. Kerzhanovich, V. I. Moroz, and M. Y. Marov (1985), Models of the structure of the atmosphere of Venus from the surface to 100 kilometers altitude, *Adv. Space Res.*, *5*(11), 3–58, doi:10.1016/0273-1177(85)90197-8.
- Stamnes, K., S.-C. Tsay, W. Wiscombe, and K. Jayaweera (1988), Numerically stable algorithm for discrete-ordinate-method radiative transfer in multiple scattering end emitting layered media, *Appl. Opt.*, *27*, 2502–2509, doi:10.1364/AO.27.002502.
- Svedhem, H., et al. (2007), Venus Express: The first European mission to Venus, *Planet. Space Sci.*, *55*, 1636–1652, doi:10.1016/j.pss.2007.01.013.
- Taylor, F. W., et al. (1980), Structure and meteorology of the middle atmosphere of Venus: Infrared remote sensing from the Pioneer Orbiter, *J. Geophys. Res.*, *85*(A13), 7963–8006, doi:10.1029/JA085iA13p07963.
- Titov, D., et al. (2006), Venus Express science planning, *Planet. Space Sci.*, *54*, 1279–1297, doi:10.1016/j.pss.2006.04.017.
- Titov, D. V., F. W. Taylor, H. Svedhem, N. I. Ignatiev, W. J. Markiewicz, G. Piccioni, and P. Drossart (2008), Atmospheric structure and dynamics as the cause of ultraviolet markings in the clouds of Venus, *Nature*, *456*, 620–623, doi:10.1038/nature07466.
- Tomasko, M. G., L. R. Doose, and P. H. Smith (1985), The absorption of solar energy and the heating rate in the atmosphere of Venus, *Adv. Space Res.*, *5*(9), 71–79, doi:10.1016/0273-1177(85)90272-8.
- Zasova, L. V., et al. (1985), VENERA-15 and VENERA-16 infrared experiment: Some spectral analysis results on the cloud structure, *Cosmic Res.*, Engl. Transl., *23*, 189–201.
- Zasova, L. V., V. I. Moroz, L. W. Esposito, and C. Y. Na (1993), SO₂ in the middle atmosphere of Venus: IR measurements from VENERA-15 and comparison to UV data, *Icarus*, *105*, 92–109, doi:10.1006/icar.1993.1113.
- Zasova, L. V., V. I. Moroz, V. M. Linkin, I. V. Khatuntsev, and B. S. Maiorov (2006), Structure of the Venusian atmosphere from surface up

to 100 km, *Cosmic Res.*, Engl. Transl., 44, 364–383, doi:10.1134/S0010952506040095.
Zasova, L. V., N. Ignatiev, I. Khatuntsev, and V. Linkin (2007), Structure of the Venus atmosphere, *Planet. Space Sci.*, 55, 1712–1728, doi:10.1016/j.pss.2007.01.011.

M. Almeida, ESA, ESAC, PO Box 78, E-28691 Villanueva De La Cañada, Madrid, Spain. (Miguel.Almeida@sciops.esa.int)

V. Cottini, NASA Goddard Space Flight Center, 8800 Greenbelt Road, Building 2, Code 693, Greenbelt, MD 20771, USA. (valeria.cottini@gmail.com)

P. Drossart, LESIA, Observatoire de Paris, Section de Meudon, place Jules Janssen 5, F-92195 Meudon CEDEX, France. (Pierre.Drossart@obspm.fr)

N. Ignatiev, Space Research Institute for Russian Academy of Sciences, Profsoyuznaya 84/32, GSP-7, 117997 Moscow, Russia. (ignatiev@irn.iki.rssi.ru)

N. Manoel, Department of Mathematics, University of Évora, Office 258, R. Romão Ramalho, 59, P-7000 Évora, Portugal. (manoix@galaxy.lca.uevora.pt)

W. J. Markiewicz and D. V. Titov, Max-Planck-Institut für Sonnensystemforschung, Max-Planck-Strasse 2, D-37191 Katlenburg-Lindau, Germany. (markiewicz@mps.mpg.de; titov@mps.mpg.de)

G. Piccioni, INAF, IASF, via del Fosso del Cavaliere 100, I-00133 Rome, Italy. (giuseppe.piccioni@iasf-roma.inaf.it)

Th. Roatsch, Institute of Planetary Research, German Aerospace Center, Rutherfordstrasse 2, D-12489 Berlin, Germany. (thomas.roatsch@dlr.de)